

This is an Open Access document downloaded from ORCA, Cardiff University's institutional repository:<https://orca.cardiff.ac.uk/id/eprint/136072/>

This is the author's version of a work that was submitted to / accepted for publication.

Citation for final published version:

Guteša, Božo, Mashruk, Syed, Zitouni, Seif-Eddine and Valera Medina, Agustin 2021. Humidified ammonia/hydrogen RQL combustion in a trigeneration gas turbine cycle. *Energy Conversion and Management* 27 , 113625. 10.1016/j.enconman.2020.113625

Publishers page: <https://doi.org/10.1016/j.enconman.2020.113625>

Please note:

Changes made as a result of publishing processes such as copy-editing, formatting and page numbers may not be reflected in this version. For the definitive version of this publication, please refer to the published source. You are advised to consult the publisher's version if you wish to cite this paper.

This version is being made available in accordance with publisher policies. See <http://orca.cf.ac.uk/policies.html> for usage policies. Copyright and moral rights for publications made available in ORCA are retained by the copyright holders.



Humidified Ammonia/Hydrogen RQL combustion in a Trigeneration Gas Turbine Cycles

Guteša Božo M^a, Mashruk S^b, Zitouni S^b, Valera-Medina A^b

^aResearch and Development Department, Termoinžinjering d.o.o, Zrenjanin, Serbia

^bCardiff School of Engineering, Cardiff University, Queen's Building, Cardiff, United Kingdom

Abstract

Ammonia is an example of a zero-carbon fuel of high interest for implementation in gas turbine technologies. Preliminary analyses showed that a basic humidified ammonia-hydrogen Brayton cycle can produce total plant efficiencies of ~34%. However, further improvements are required to make these units competitive to current fossil-based plants whose efficiencies are above 80%. Thus, this work seeks to numerically and analytically demonstrate the implementation of a complex cycle that will increase final efficiencies whilst using the full potential of ammonia as a cooling fluid, power fuel and heating gas (i.e. trigeneration cycle) with heat district distribution. Therefore, a basic gas turbine cycle was inserted into a two-shaft, reverse Brayton gas turbine plant facility. In order to improve combustion and reduce emissions, a Rich-Quench-Lean system was integrated into the analysis by resolving the combustion performance via CHEMKIN-PRO. Detailed sensitivity analyses were also conducted throughout the burner to identify the key reactions responsible for both flame stability and NO formation/reburn, which are vital for future safe and efficient operation of these types of cycles. The study shows that the total efficiency has significantly increased when compared to the basic turbine facility, with a value ~59%. Moreover, low emissions were accomplished below current European NO_x thresholds. The obtained values show a significant potential for the utilisation of ammoni-based blends with steam injection in gas turbine facilities through employment of novel cycles that consider lower dilution in the combustion sector in combination with novel ammonia combustion systems and trigeneration concepts.

Keywords: Novel cycles, humidified gas turbines, ammonia/hydrogen, trigeneration, combined heat power and cooling, RQL

1. Introduction

Ammonia has recently gained considerable attention, with organisations such as the International Energy Agency [1] recognising it as a potential fuel for future applications. Ammonia, under assessment for more than 60 years [2], is one of the world's most produced chemicals, with an entrenched and well-recognised production, transportation and storage infrastructure. The thermal properties of Ammonia,

with respect to boiling temperature and liquefaction pressure, allow storage in liquid form at about 8.5 bar (at standard room temperature), or cooled to $-33\text{ }^{\circ}\text{C}$ (at atmospheric pressure) [3,4]. As such, it is now being considered for commercial applications, in the power industry, and as fuel in marine transportation [5], denoting the fast improvement in the understanding of the use of ammonia, in terms of both combustion and storage properties. However, further investigation is required, for ammonia to be fully accepted as one of the supporting pillars of a zero-carbon energy transition. Challenges to full global deployment range from a lack of understanding of fundamental combustion characteristics, particularly under turbulent conditions, and the complexity of nitrogen bounding reactions [5–8], to the economic repercussions of the introduction of ammonia into the global energy mix [9,10]. Amongst these topics, the efficient use of ammonia for power generation, at medium and large power scale is critical for the success of this technology and use of the molecule in real industrial applications.

Although considerable research has been dedicated to the utilisation of ammonia in internal combustion engines [11–14], the use of the molecule as a viable energy source in gas turbines has only recently re-emerged over the last half decade. Historically, during the Second World War, complex development programs were undertaken, mostly driven by the United States Army [15]. Although initial results were encouraging, confirming that the use of ammonia at 2.35 times the rate of diesel would result in cooler turbine temperatures for a given power output and a gain in power output between 9 and 13% with thermal efficiency increase of $\sim 2.5\%$ [16], the increase in ammonia mass flowrates compared to hydrocarbons made the technology uncompetitive, thus leading to the end of the program in an expanding carbon-based economy.

However, growing concern over the detrimental environmental impact associated to carbon-based fuel combustion have re-ignited interest around hydrogenated molecules such as ammonia. Being carbon-free, ammonia can provide the medium for storage of stranded energy (wind, solar, tidal) whilst ensuring chemical stability for the use of this energy over long periods of time (i.e. years). Consequently, works on the use of methane-ammonia [17, 18], Coke Oven Gas-ammonia [19], ammonia-hydrogen [20–22] and pure ammonia [23–25] have been undertaken, in an attempt to assess the feasibility of ammonia as a means of reducing/eliminating carbon in gas turbine power production. Most studies have focused on the complex reaction mechanisms, flame structures and technical challenges of using the molecule for these means of energy generation. However, just a few have attempted to determine an efficient method for the utilisation of ammonia [21, 26]. The main need for these studies is that practical requirements and industrial interest can only be attracted once efficient, profitable systems can be implemented.

One proposal that has been continuously presented to support the efficient use of ammonia in gas turbines is the use of multi-stage combustion systems. The implementation of these units can enable full recovery of molecular stored energy whilst ensuring low NO_x emissions, one of the major associated

obstacles of using ammonia as a fuel. One solution is the development of Rich-Quench-Lean (RQL) technologies [27]. The system, based on multi-staged combustion at different equivalence ratios, permits the reduction of emissions whilst increasing stability in the primary combustion zone [28, 29]. The high hydrogen content in the post-combustion of ammonia rich flames, observed by many [22, 26, 30], has inclined researchers and developers into the use of the technology for ammonia combustion [22, 25]. Hence, this technique will be evaluated in this work as part of the integration of a novel cycle.

Moreover, an additional manner to augment power and efficiency is to employ humidified cycles that enable the increase of mass through the system [31]. Cycles of gas turbines with steam injection have been studied and improved over the years [32, 33], especially for Combined Heat and Power (CHP) and Combined Cooling, Heat and Power (CCHP) configurations [34]. Humidification has also been employed in systems integrated with steam reforming [35, 36] and at different compressor stages [37], thus showing great versatility. However, humidified regimes need to be carefully understood to avoid combustion and ignition problems [38]. Once the limits of steam injection are known and their effects on the flame/combustion process minimized, the method can be effectively implemented in CCHP units while making use of cooling and heating properties of various streams, thus optimising energy consumption and enabling operation under off-design conditions [39, 40]. Steam injection in a cycle is considered to be an optimal way for the recovery of waste heat [41]. In addition, reduction of nitrogen oxide emissions is about 1.7 times more efficient when steam injection is applied compared to humidity increase in the inlet air [42], while in the case of the hydrogen-based mixtures the inhibiting effect of dilution by steam injection when the nitrogen oxides are formed is stronger at high flame temperatures [43]. Therefore, steam injection in combination with recirculation of other combustion products can improve the efficiency of gas turbines and their specific fuel consumption. When steam injection is applied into the combustion chamber the gas turbine specific work is enhanced about 3% for every 2% increase of steam/air ratio [44].

Finally, all these concepts can be combined using various molecules cooling, heating and power properties, thus providing a great variety of combinations including those applicable features to gas turbine plants. Large scale CCHP systems are often a combination of gas turbine and steam turbines. These configurations are usually set up to support district heating/cooling demand with improvements on energy saving as well as carbon dioxide emissions reduction [39]. Combinations of Rankine cycles, organic Rankine cycles (ORC) and gas turbines in triple combined systems can deliver 47.65% thermal efficiency [45]. Considering the total heat input from the fuel in the burner, the power production of the GT-rORC combined cycles can be increased up to 40.7% [46]. On the other hand, CHP and CCHP systems can combine gas turbines with heat recovery steam generators (HRSG) [35]. CHP systems with both gas turbines and HRSG can obtain efficiencies about 82% [47], whilst CCHP systems based on gas turbines and utilization of waste heat for heat energy production and cooling can reach efficiency

outputs of up to ~82-85% [48]. Further studies have explored the idea of using a CCHP configurations that includes two shafts double Brayton cycle (Brayton and reversed Brayton cycle) with the combustion of natural gas and recirculation of carbon dioxide. These configurations have shown efficiencies of ~52.3% [49].

However, to date, no research exists to show the effect of humidified conditions on CCHP cycles operating on ammonia-based fuels with RQL technology. As mentioned before, efficiency and power output of ammonia-based cycles can be increased by implementation of all these techniques. This step ensures improved economics for the use of ammonia. Combustion analyses of ammonia blends doped with hydrogen in gas turbines with the implementation of humidification are quite limited, thus requiring a study such as this to determine the feasibility of implementing a more comprehensive cycle with novel ammonia combustion methods capable of recovering as much energy as possible while minimizing unwanted emissions from such a chemical. Therefore, this work analyses such a novel cycle using the above-mentioned advanced combustion systems. The results are approached in terms of the chemistry of various molecules during the combustion of a proposed humidified blend, their impact on the cycle and the final thermodynamic analytics of a novel CCHP cycle to recover as much energy as possible from ammonia, thus competing with carbon based-fuelled industrial systems. The model applied for cycle calculations has been previously validated for a real gas turbine [49], with relative errors under 5%, most under 2%. It is emphasised that the results discussed in this study cannot be validated experimentally, since units of this magnitude running on ammonia blends do not exist. Thus, all the following results are for guidance to develop such systems at efficiencies as high as those presented by fossil fuel running cycles.

2. Methods and Materials

2.1. Numerical Combustion Analysis

A chemical kinetic modelling tool, CHEMKIN-PRO was utilised to model chemical kinetics of the problem at hand. The PREMIX reactor [50] and the Equilibrium tool [51] were used to calculate the laminar flame speed (S_L) and adiabatic flame temperature (AFT), respectively. Solutions in this program were based on an adaptive grid of 1000 points, with mixture-averaged transport properties and trace series approximation. The calculation employed the NH_3 reaction mechanisms from Xiao et al. [52], comprised of 55 chemical species and 276 reactions. These results were used to model the RQL burner in the CHEMKIN-PRO environment.

A Chemical Reactor Network (CRN) was also developed, based on representative combustion geometry [54, 55] to model the RQL burner in the CHEMKIN-PRO environment, schematically presented in Fig. 1, to numerically determine the species obtained from rich swirling flame followed by after-

lean return. Mixing zone, flame zone, Central Recirculation Zone (CRZ) and External Recirculation Zone (ERZ) were modelled by individual perfectly stirred reactors (PSR) and the residence time for each PSR was obtained from RANS CFD analysis [56]. The recirculation strength was determined by previous experimental campaigns employing comparable burners [57, 58] and mass recirculation percentages for the PSR network are shown in Fig. 1. The calibration of the model for determination of heat losses in the rich burning zone was achieved in accordance to previous experiments [20, 58, 59]. The outlet from the flame zone fed a Plug Flow Reactor (PFR) to simulate reactions in the post-flame zone. The quenching/mixing zone where the products from a rich swirling flame and secondary air mixes was modelled by a partially stirred reactor (PaSR) and the lean burning zone afterwards was modelled by another PFR. The number of Monte Carlo Simulation samples (NPAR) for the PaSR was chosen at 200 since this value provides a reasonable balance between accuracy and execution time. The reaction mechanism from Xiao et al. [53] was relied upon to predict species formation through the system, with results from this reactor modelling were used in the cycle analysis. For this study, the blend that was employed was set to 70-30 (vol%) $\text{NH}_3\text{-H}_2$ under humidified conditions at an equivalence ratio (ER) of 1.2. The 70-30 (vol%) ratio of $\text{NH}_3\text{-H}_2$ have demonstrated favourable stability in previous work [22] and shown to exhibit comparable behaviour to $\text{CH}_4\text{-air}$ flame [60]. This choice of ER has been shown to produce best results with respect to emission values in previous numerical and experimental campaigns [21, 22]. Simulations were performed with inlet temperature of 560K and a pressure of 9.67 bar, with fuel and steam flow of 0.367 and 0.147 kg/s, respectively and a secondary air flow of 6.7 kg/s at 960 K temperature. Selection of these flow conditions are discussed in detail in the following section.

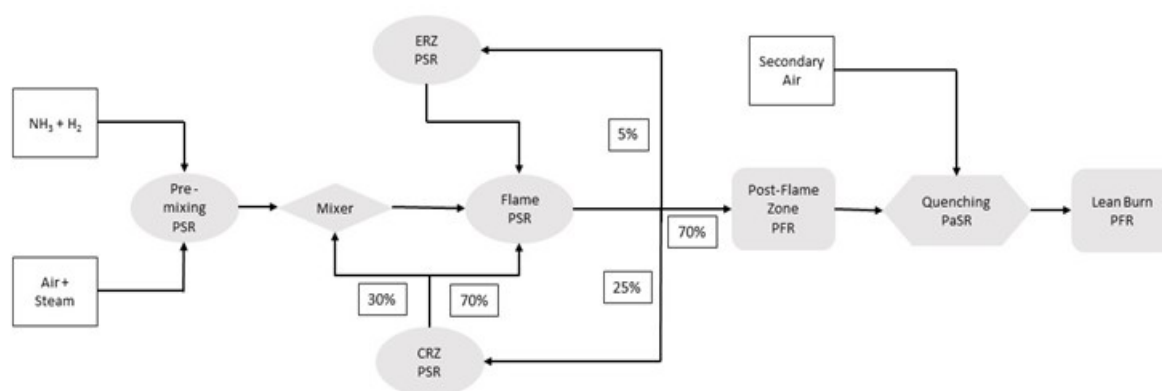


Fig 1. Chemical reaction network

2.2. Basic Humidified Brayton cycle

Analyses were conducted using a calibrated mathematical model developed for regular Brayton natural gas cycles that operate under designed and off-designed regimes. The model has been also successfully correlated (i.e. with ASPEN results) and used for analysis of combustion of oxygen-methane in combination with an innovative working fluid blend (i.e. CO₂/argon/steam - CARSOXY) [61]. The hypothesis behind the model was its potential use in more complex fuel blends, such as the ones formed by combination of gasification gas from corn-cob and natural gas [50].

The applied model considers adiabatic expansion processes with cooling of the turbine blades. The selected 'reference method' is based on the assumption that cooling air is continually distributed through gas. The expansion process of the combustion products and expansion of cooling air are calculated separately. For the numerical model, adjustments were necessary, therefore the effects of water vapor and fuel enthalpy impacts to match real gas turbine plants were included. Further details can be found elsewhere [62]. The high accuracy of the method was previously demonstrated by comparing various predicted parameters with results from manufacturers' reports, with relative errors under 5% [63]. For analyses conducted on the humidified ammonia blend, the model employed predicted the inlet parameters. The model was applied to determine the efficiency of the ammonia/hydrogen cycle with humidification and RQL combustion. Initially, the power output of the cycle was determined. Assumed inlet parameters values for basic humidified Brayton cycles are presented in Table 1.

Table 1. Inlet parameters values for basic humidified Brayton cycle

Parameter	Symbol	Value	Unit
Ambient pressure	p_o	0.10	MPa
Ambient temperature	T_o	280	K
Air mass flow for sealing relative to air mass flow at the compressor inlet	z	0.01	-
Compressor pressure ratio	Π_c	10.2	-
Polytropic efficiency of a compressor	$\eta_{p c}$	0.80	-
Combustion chamber pressure ratio	Π_{cc}	0.97	-
Efficiency of a combustion chamber	η_{cc}	0.90	-
Gas turbine inlet temperature	T_3	1265	K
Polytropic efficiency of a turbine	$\eta_{p T}$	0.85	-
Mechanical efficiency	η_m	0.90	-
Cooling air mass flow specified to compressor inlet mass flow	r_{air}	0.035	kg/kg

Cooling air distribution factor	M	0.667	-
Ratio of the vapor mass flow and fuel mass flow at the combustion chamber inlet	α	0.40	-
Air mass flow rate at the compressor inlet	m_1	9.280	kg/s
Air mass flow rate at the compressor outlet (combustion chamber inlet)	m_2	8.960	kg/s
Air mass flow rate for cooling gas turbine blades	m_{air}	0.325	kg/s
Fuel mass flow rate	m_{fuel}	0.367	kg/s
Steam mass flow rate	m_{steam}	0.147	kg/s
Combustion products mass flow rate at the turbine inlet	m_3	9.474	kg/s
Combustion products mass flow rate at the turbine outlet	m_4	9.891	kg/s

Due to the limits of the calibration, fuel flow rates were restricted; therefore, an inlet fuel flowrate of 0.367 kg/s was set using a 70-30% NH₃-H₂ (vol%) blend. The value of the steam flowrate was set at 0.147 kg/s in accordance with the reference gas turbine plant that uses a steam/fuel ratio of 0.4 kg/kg_{fuel}. The equivalence ratio was determined at 1.2 with 2.260 kg/s of air in order to obtain rich conditions across the combustion process. These conditions delivered 10.45 MW of supplied heat. The atmospheric pressure and temperature adopted in the study were 1 bar and 288K, respectively. The compressor pressure ratio was set at 10.2 with a polytropic efficiency of 80%. The combustion chamber pressure drop was 3%, with combustion efficiencies of 90%. The turbine polytropic efficiency was set at 85%, with mechanical losses of 10%. For inlet turbine temperatures, the values used were obtained from the preliminary numerical assessment, Section 3.1.

2.3. Ammonia trigeneration cycle

The basic gas turbine cycle was introduced into a two-shaft gas turbine plant facility consisting of a basic humidified Brayton cycle and a reversed Brayton cycle with steam generation for its addition to the combustion chamber, fuel preheating and ammonia-cooled inlet air at the compressor, Fig 2, thus truly working as a trigeneration cycle that employs all benefits from ammonia.

After combustion of the blend and expansion in the gas turbine, combustion products are introduced into a second gas turbine as a part of the reversed Brayton cycle. Exhaust gases with high temperatures and humidity and at atmospheric pressure (from the outlet of the first gas turbine) are used for the production of additional power from the expansion to negative pressures in the turbine. The gas mixture is still a high-temperature fluid at the end of the second expansion, hence needing to be cooled. The gas mixture is cooled down by applying a special regenerative heat exchanger (HE1).

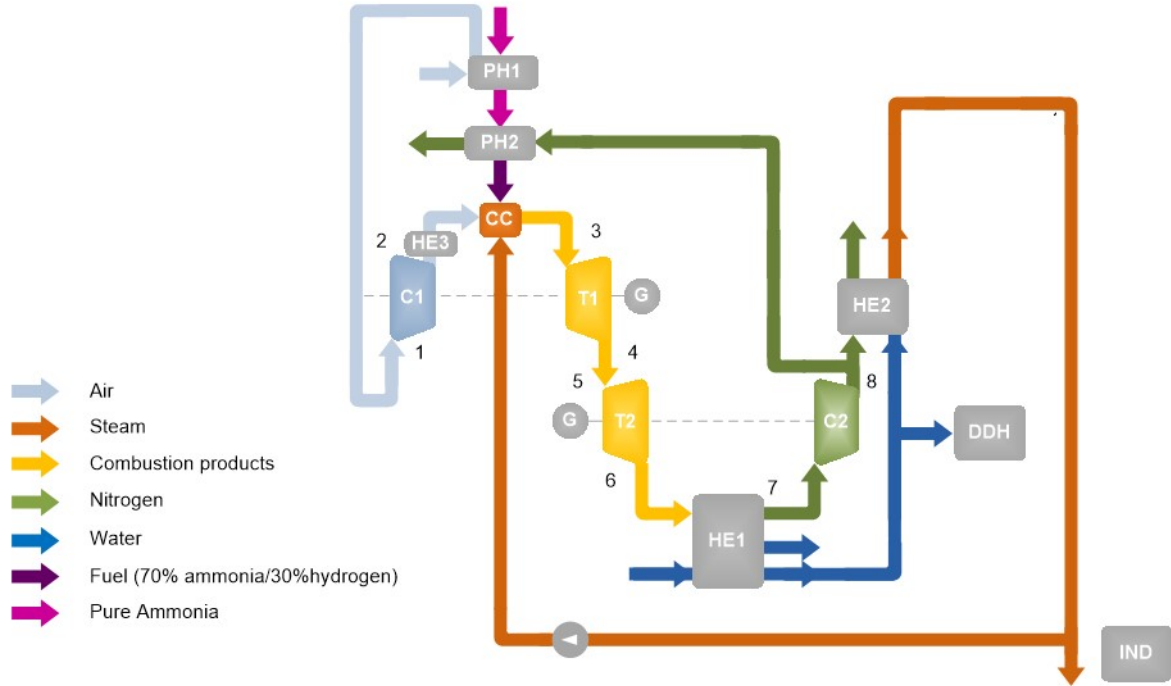


Fig 2. Ammonia trigeneration cycle

Steam is transformed to condensate and extracted from the mixture. The pressure of the gas is lower than the atmospheric pressure, hence it is compressed in a second compressor to atmospheric pressure. The compressed gas is employed for fuel preheating before introducing this fuel back into the combustion chamber, while steam is also injected in the latter. The excess heat from the compressed gas is used for preparation of warm water for district heating or for other applications (which are not taken into consideration in the final efficiency calculations). Meanwhile, the ammonia expansion (from liquid to gas state) is used for cooling the air which is then compressed in the first compressor. Gaseous ammonia is further heated by hot nitrogen. The specific compression work for the humidified Brayton cycle is analysed as adiabatic and polytropic. Calculations of the specific off-design compression work are done as a function of compressor pressure ratio, inlet temperature and specific heat [62]. The combustion air and the air for cooling the gas turbine are both compressed. Continuous distribution of the air for cooling of the gas turbine is assumed. The overall cycle efficiency in the case of the humidified gas turbine Brayton cycle is calculated by the following equation,

$$\eta_{HB} = \frac{(L_T \cdot \eta_m - L_C)}{q_{sup}} \quad (1)$$

Where η_{HB} is the overall efficiency [-] and η_m the mechanical efficiency [-]. Combustion products are further expanded in the second gas turbine as a part of the reversed Brayton cycle. The expansion in the

second turbine is analysed as an adiabatic expansion without turbine blades cooling. Combustion products, after the second expansion, are introduced into the heat exchanger 1 (HE1). For this heat exchanger an efficiency η_{HE} is assumed. The exchanged heat flux is calculated as,

$$\dot{m}_8 \cdot \eta_{HE} \cdot (h_{HEin} - h_{HEout}) = \dot{m}_w \cdot (h_{wout} - h_{win}) \quad (2)$$

where m_8 is the mass flow of the combustion products after the second expansion in the inversed Brayton cycle, h_{HEin} is the combustion products enthalpy at the exchanger inlet, h_{HEout} is the combustion products enthalpy at the exchanger outlet, η_{HE} is the heat exchanger efficiency, m_w is the mass flow rate of the water for steam preparation, h_{wout} is the enthalpy of the water for steam preparation at the outlet of the exchanger and h_{win} is the water enthalpy at the inlet of the exchanger.

During the heat exchange process in HE1, gaseous nitrogen is extracted from the combustion products and introduced in the second compressor as part of the reversed Brayton cycle. The specific compression work for gaseous nitrogen in the reversed Brayton cycle is calculated by the following equation,

$$L_{C2} = c_{p_{N2}} \Big|_7^8 \cdot T_7 \cdot \left(\Pi_C^{(1/\eta_{pC}) \cdot (R_{N2}/c_{p_{N2}} \Big|_7^8)} - 1 \right) \quad (3)$$

Fuel is preheated in two steps. The first step preheats the liquid ammonia with air before the compression in the humidified Brayton cycle. In this step, air is cooled from 15°C to 7°C before introducing it into the compressor. Then, liquid ammonia is preheated in the preheater in the preheater 1 (PH1). The heat flux, with the assumed value of the preheater efficiency η_{PH} , is calculated as,

$$\dot{m}_2 \cdot \eta_{PH} \cdot (h_{PHin} - h_{PHout}) = \dot{m}_{NH3} \cdot (h_{NH3-1out} - h_{NH3-1in}) \quad (4)$$

where m_2 is the mass flow rate of the cool air before accessing the compressor in the humidified Brayton cycle, h_{PHin} is the enthalpy of the air at 15°C at the preheater inlet, h_{PHout} is the air enthalpy at 7°C at the preheater outlet, η_{PH} is the preheater efficiency, m_{NH3} is the liquid ammonia flow rate, $h_{NH3-1out}$ is the enthalpy of the heated ammonia at the preheater outlet and $h_{NH3-1in}$ is the liquid ammonia enthalpy at the preheater inlet.

The second step of fuel preheating heats up the gaseous ammonia with hot gaseous nitrogen from the second compressor from the reverse Brayton cycle. Gaseous ammonia is preheated in the preheater 2 (PH2), where it is assumed that hydrogen is produced via catalytic reactors and heat from the hot nitrogen stream. The heat flux, with efficiency η_{PH} , is calculated as,

$$\dot{m}_{N2} \cdot \eta_{PH} \cdot (h_{PHin} - h_{PHout}) = \dot{m}_{NH3} \cdot (h_{NH3-2out} - h_{NH3-2in}) \quad (5)$$

where m_{N2} is the hot gaseous nitrogen flow rate from the second compressor in the reversed Brayton cycle, h_{PHin} is the enthalpy of the gaseous nitrogen at the preheater inlet, h_{HEout} is the gaseous nitrogen

enthalpy at the preheater outlet, η_{PH} is the preheater efficiency, m_{NH_3} is the liquid ammonia flow rate, h_{NH_3-2out} is the enthalpy of the heated ammonia at the preheater outlet and h_{NH_3-2in} is the enthalpy of the liquid ammonia at the preheater inlet.

After HE1, hot water for steam preparation is heated in HE2 by the excessive hot nitrogen from the second compressor outlet. The heat flux, with the efficiency η_{HE} , is calculated as,

$$(\dot{m}_8 - \dot{m}_{N_2}) \cdot \eta_{HE} \cdot (h_{HEin} - h_{HEout}) = \dot{m}_w \cdot (h_{wout} - h_{win}) \quad (6)$$

where $(m_8 - m_{N_2})$ is the hot nitrogen mass flow rate that remains after removing hot nitrogen for fuel preheating, h_{HEin} is the hot nitrogen enthalpy at the exchanger inlet, h_{HEout} is the hot nitrogen enthalpy at the exchanger outlet, η_{HE} is the heat exchanger efficiency, m_w is the water mass flow rate for steam preparation, h_{wout} is the water enthalpy for steam preparation at the exchanger outlet and h_{win} is the water enthalpy at the exchanger inlet.

The generated steam from HE is further introduced into the pump for pressure increase. Calculation of the pump power is done using the formula,

$$P_{pump} = \dot{m}_{pump} \cdot \eta_p \cdot (h_{pout} - h_{pin}) \quad (7)$$

where m_{pump} is mass flow rate of the injected water, η_p is mechanical efficiency of the pump, and h_{pin} , h_{pout} are the water enthalpy at pump inlet and pump outlet, respectively.

Compressed air at the outlet of the compressor is cooled down to 560 K, as the requirement of the combustion chamber, in the heat exchanger 3 (HE3). The heat flux, with the efficiency η_{HE} , is expressed as,

$$\dot{m}_{air} \cdot \eta_{HE} \cdot (h_{HEin} - h_{HEout}) = \dot{m}_w \cdot (h_{wout} - h_{win}) \quad (8)$$

where m_{air} is the compressed air mass flow rate at the compressor outlet, h_{HEin} is the air enthalpy at the exchanger inlet, h_{HEout} is the air enthalpy at the exchanger outlet, η_{HE} is the assumed heat exchanger efficiency, m_w is the cooling water mass flow rate, h_{wout} is the enthalpy of the water at the exchanger outlet and h_{win} is the enthalpy of the water at the exchanger inlet. The thermodynamic parameters of each point defined in Figure 2 are given in the Figure 3.

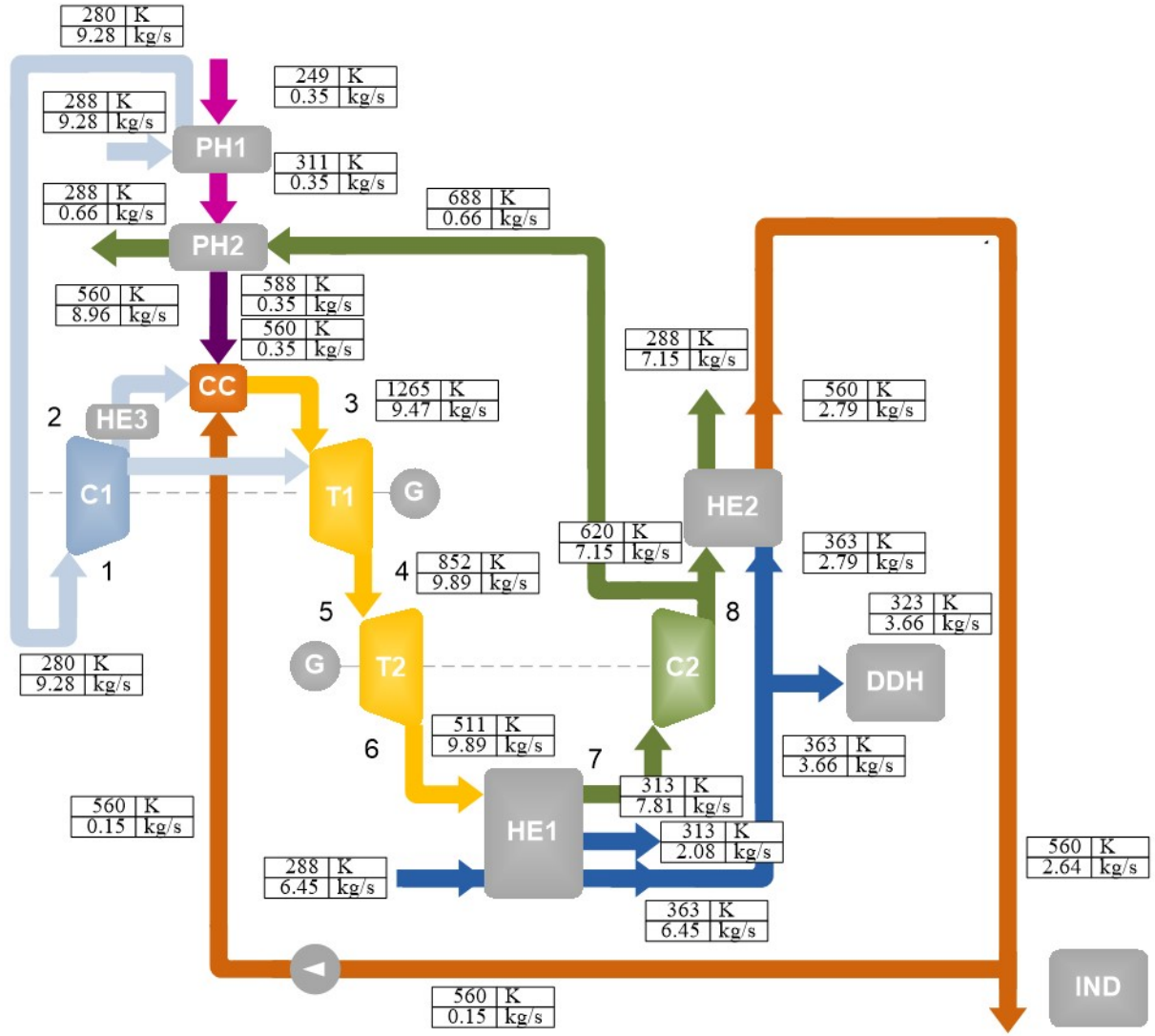


Fig 3. Ammonia trigeneration cycle with thermodynamic parameters

The trigeneration cycle efficiency is calculated as the ratio of a sum of all gained and invested power in the cycle to the supplied power from the fuel. The overall efficiency of the trigeneration cycle is calculated by the equation,

$$\eta_{TC} = \frac{(P_G \cdot \eta_m - P_I)}{q_{sup}} = \frac{((P_{T1} + P_{T2} + P_{DDH}) \cdot \eta_m - (P_{C1} + P_{C2} + P_{pump} + P_{H2}))}{q_{sup}} \quad (9)$$

Where η_{TC} is the efficiency of the overall trigeneration gas turbine cycle [-], η_m is the mechanical efficiency [-], P_G is the overall gained power in the cycle [kW], P_I is the overall invested power in the cycle [kW], Q_{sup} is the supplied power to the cycle from the fuel [kW], P_{T1} is the power produced in the gas turbine in the humidified Brayton cycle [kW], P_{T2} is the power from the gas turbine in the reversed Brayton cycle [kW], P_{DDH} is the heat power for district heating water preparation [kW], P_{C1} is the power

needed for compression of air in the humidified Brayton cycle [kW], P_{C2} is the power needed for compression of gaseous nitrogen in the reversed Brayton cycle [kW], P_{pump} is the power required for the steam pump [kW] and P_{H2} is the heat power for hydrogen preparation [kW].

3. Results and Discussion

3.1. Numerical Results from the CRN

Table 2 displays the combustion results at the different sections of the RQL combustion system, fuelled by humidified 70/30 NH_3/H_2 blend. Significant amount of ammonia remains unburnt in the rich flame zone, which get nearly burnt out at the lean burn zone. Compared to ammonia, significant amount of hydrogen remained unburnt at the lean burn zone, thereby keeping specific heat of combustion products at the required level. Temperature of the flame increases significantly at the post flame zone. Then reduced to the required turbine entry temperature by mixing with considerably cooler secondary air at the quenching zone. Water vapour mole fraction increased at the post flame zone, then reduced at the quenching zone due to air addition and then increased again at the lean burn zone due to increase in the temperature. Substantial amount of NO_x is generated at the flame zone as high amount of ammonia burns here. However, these NO_x burns away as the flame progresses at different zones. Normalised NO_x emissions (which have been normalised to 15% oxygen in accordance with British standards [64]) were obtained. At the end of the process, ~99.83% of the final products are mainly water, oxygen and nitrogen. Detailed sensitivity analyses of the species of interest at different zones is carried out at the later part of this work.

3.1.1. Sensitivity Analyses

Sensitivity analyses on net reaction rate has been carried out for important contributing radicals in the combustion process, namely H, O, OH and NH_2 at different locations of the RQL combustor. H, O and OH radicals significantly increase the reaction rate of ammonia/hydrogen burning through various reactions, especially $H + O_2 \leftrightarrow O + OH$; $O + H_2 \leftrightarrow H + OH$ and $OH + H_2 \leftrightarrow H + H_2O$, Fig 4. NH_2 radical is of particular interest for ammonia burning as NH_3 converts to NH_2 radicals initially, prior to further reduction. Fig. 5 displays $[NH_2]$ sensitivity coefficients at different locations of the burner.

Fig. 4 compares the normalized sensitivity coefficients of H, O and OH radicals at the flame zone, post flame zone and lean burn zone. The chain branching reaction $H + O_2 \leftrightarrow O + OH$ is one of the most important elementary reactions in combustion that provides the necessary OH and O radicals in any hydrogen-based flame. At the flame zone, OH radicals react with ammonia molecules to produce NH_2 radicals and water, whereas O radicals reduce NH_3 through the reaction $NH_3 + O \leftrightarrow NH_2 + OH$. The

third body reaction $\text{NH}_3 + \text{M} \leftrightarrow \text{NH}_2 + \text{H} + \text{M}$ also produce NH_2 radicals from ammonia. This NH_2 radicals in turn react with H_2 molecules to produce H radicals. Some of the NH_2 radicals convert to NH_3 and NH radicals through the decomposition reaction $2\text{NH}_2 \leftrightarrow \text{NH}_3 + \text{NH}$, Fig. 5. The NH radicals react with available O_2 at the flame front to produce HNO, which in turn converts to NO by reacting with H radicals through the reaction $\text{HNO} + \text{H} \leftrightarrow \text{NO} + \text{H}_2$. Furthermore, NO reacts with NH_2 radicals to produce NNH and OH radicals.

Table 2. Results from CHEMKIN-PRO applied to the RQL system

Mechanism	Xiao			
	Flame Zone	Post Flame Zone	Quenching / Mixing Zone	Lean Burn Zone
Temperature (K)	1624	2169	1196	1265
NH_3 mole fraction	9.30E-02	5.30E-06	1.22E-06	3.30E-07
H_2 mole fraction	2.14E-02	5.00E-02	1.15E-02	1.90E-03
O_2 mole fraction	5.14E-02	4.01E-06	1.62E-01	1.58E-01
H_2O mole fraction	2.32E-01	3.28E-01	7.53E-02	8.54E-02
H mole fraction	7.15E-05	3.43E-04	7.89E-05	7.63E-07
O mole fraction	1.35E-05	1.44E-06	3.32E-07	5.21E-06
OH mole fraction	6.28E-05	3.36E-04	7.71E-05	1.45E-05
NH_2 mole fraction	9.68E-04	1.12E-07	2.57E-08	3.53E-09
N_2 mole fraction	0.59374	0.62130	0.75123	0.75493
NO mole fraction	1.11E-03	3.12E-04	7.18E-05	3.76E-05
N_2O mole fraction	6.08E-03	2.28E-08	5.23E-09	8.84E-08
NO_2 mole fraction	7.55E-06	5.15E-09	1.18E-09	3.54E-05
NO (ppmv)	1442	465	78	41
NO_x (ppmv)	9372	465	78	80
NO – 15% O_2 (ppmv)	605	133	133	66
NO_x – 15% O_2 (ppmv)	3930	133	133	127

At the post flame zone, H radicals are mainly being produced by consuming OH and O radicals through the reactions $\text{OH} + \text{H}_2 \leftrightarrow \text{H} + \text{H}_2\text{O}$ and $\text{O} + \text{H}_2 \leftrightarrow \text{H} + \text{OH}$. Atomic nitrogen reacts with NO produced at the flame zone to produce molecular nitrogen and O radicals. Thus, this reaction has positive sensitivity for H, O and OH radicals while shows negative sensitivity for NH_2 radicals. Interestingly, NH_2 radicals are mainly consumed at the post flame zone by reacting with NO through the reactions $\text{NH}_2 + \text{NO} \leftrightarrow \text{NNH} + \text{OH}$ and $\text{NH}_2 + \text{NO} \leftrightarrow \text{N}_2 + \text{H}_2\text{O}$. The former reaction is chain branching, while the latter is chain terminating, and thus NO formations are very sensitive to the branching ratio of these two reactions [7]. NO is also reduced by reacting with N and NH through the reactions $\text{N} + \text{NO} \leftrightarrow \text{N}_2 + \text{O}$ and $\text{NH} + \text{NO} \leftrightarrow \text{N}_2\text{O} + \text{H}$. The third body chain terminating reaction $\text{H} + \text{OH} + \text{M} \leftrightarrow \text{H}_2\text{O} + \text{M}$ also

plays an important role for H and OH radicals' consumption. Significant amount of HNO formed in the flame zone convert to NH radicals through reaction $\text{NH} + \text{OH} \leftrightarrow \text{HNO} + \text{H}$, operating at reverse direction.

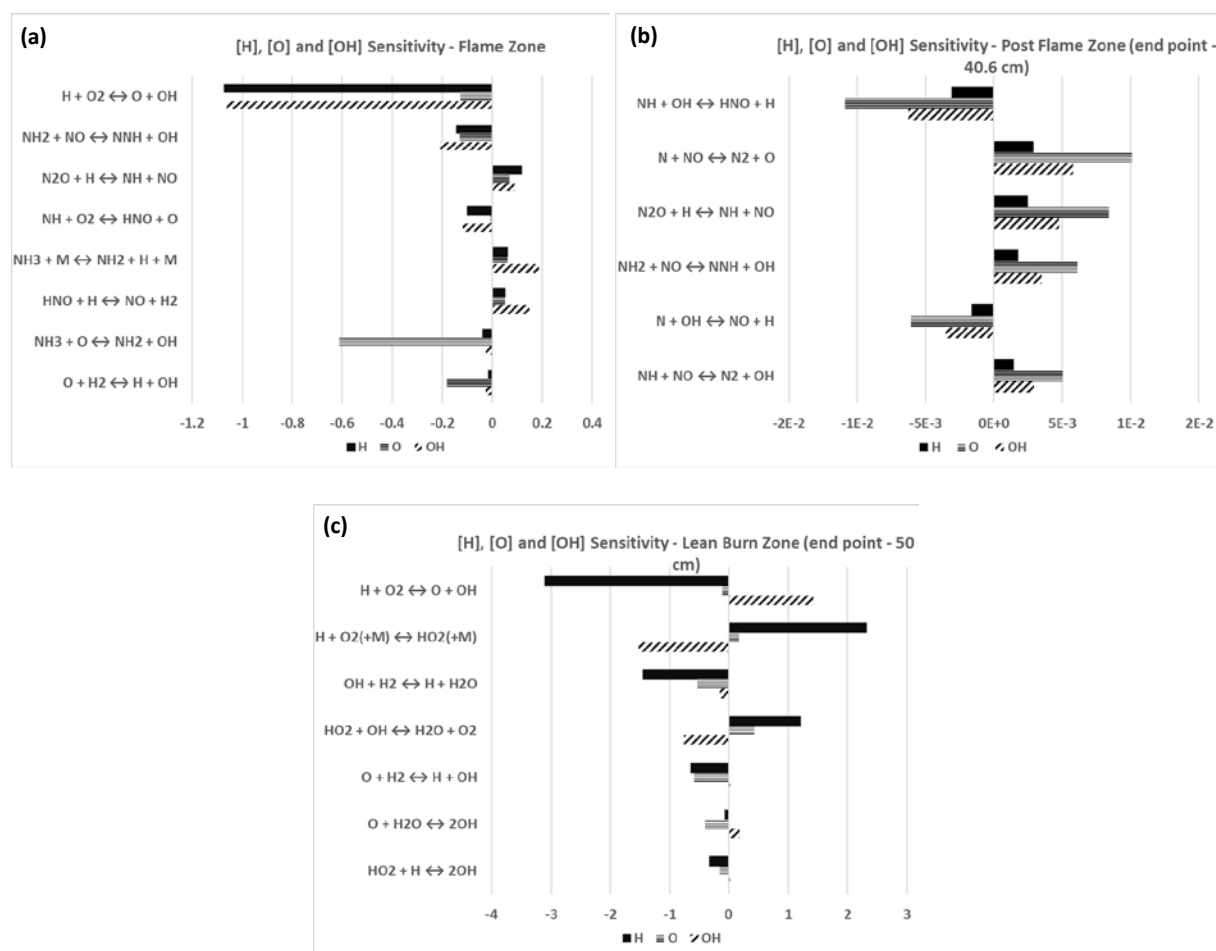


Fig 4. Computed normalized sensitivity coefficients of [H], [O] and [OH] at the (a) rich flame zone, (b) end point of post flame zone, and (c) end point of lean burn zone.

Impact of excess oxygen is clearly visible in the sensitive reactions responsible for net [H], [O], and [OH] at the lean burn zone, Fig. 4(c). The remaining hydrogen molecules convert to H and OH radicals through the reactions $\text{OH} + \text{H}_2 \leftrightarrow \text{H} + \text{H}_2\text{O}$ and $\text{O} + \text{H}_2 \leftrightarrow \text{H} + \text{OH}$, whereas excess O_2 produce O and OH radicals through the reaction $\text{H} + \text{O}_2 \leftrightarrow \text{O} + \text{OH}$. The third body reaction $\text{H} + \text{O}_2(+\text{M}) \leftrightarrow \text{HO}_2(+\text{M})$ produce hydroperoxyl radicals, which reacts with some of the OH and O radicals to convert back to O_2 through the reactions $\text{HO}_2 + \text{OH} \leftrightarrow \text{H}_2\text{O} + \text{O}_2$ and $\text{HO}_2 + \text{O} \leftrightarrow \text{OH} + \text{O}_2$, respectively. The remaining NH_3 at the lean burn zone converts to NH_2 by reacting with OH and O radicals, Fig. 5(c). Some of the

NH_2 radicals convert back to NH_3 by reacting with H_2 and produce H radicals in the process. NH_2 radicals mainly convert to aminooxidamide radicals by reacting with hydroperoxyl radicals through the reaction $\text{NH}_2 + \text{HO}_2 \leftrightarrow \text{H}_2\text{NO} + \text{OH}$ and produce OH radicals in the process.

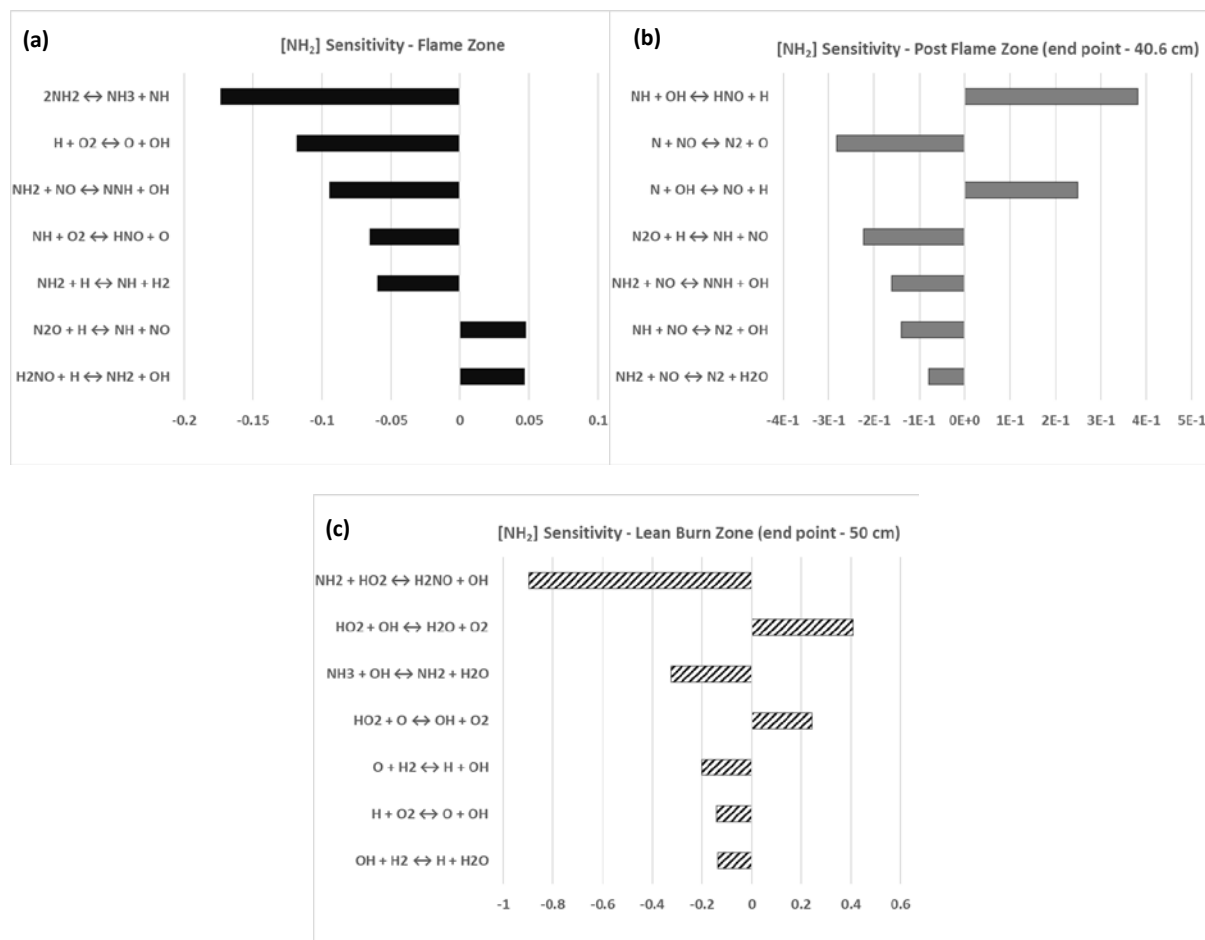


Fig 5. Computed normalized sensitivity coefficients of $[\text{NH}_2]$ at the (a) rich flame zone, (b) end point of post flame zone, and (c) end point of lean burn zone.

Absolute rate of production/consumption for H_2 and NH_3 are compared at the rich flame zone, post flame zone and lean burn zone in Fig. 6. At the flame zone, H_2 degrades to H radicals by reacting with OH, O and NH_2 radicals, Fig. 6(a). Similarly, NH_3 converts to NH_2 radicals by reacting with OH and O radicals, Fig. 6(d). As discussed earlier, major source of NO production at the flame zone are from HNO, this process also converts H radicals to H_2 molecule. The degradation process of NH_2 radicals, $\text{NH}_2 > \text{NH} > \text{N}$ also produce further hydrogen molecules. The major source of ammonia formation in the flame zone are from NH_2 radicals reacting with H_2 , and through the reaction $2\text{NH}_2 \leftrightarrow \text{NH}_3 + \text{NH}$. It must be noted that NH_3 consumption at the flame zone is more than double, compared to H_2 consumption.

At the post flame zone, H_2 and NH_3 are mostly being consumed, rather than being produced, Fig. 6(b) and (e). Hydrogen consumption rate at the post flame zone is five orders of magnitude lower than flame zone, while ammonia consumption rate is seven orders of magnitude lower. This may be attributed to two factors. Firstly, most of the fuel is being burned in the flame zone and secondly, as detailed in Section 2.1, flame zone was modelled by 0-D PSR while post flame zone was modelled by 1-D PFR, giving the ROP axially at the post flame zone and Fig. 6(b) and (e) only illustrates ROP at the end point of the PFR. Interestingly, the reactions $HNO + H \leftrightarrow NO + H_2$; $NH_2 + H \leftrightarrow NH + H_2$ and $NH + H \leftrightarrow N + H_2$ operate at reverse direction at the post flame zone. This can be attributed to increased availability of NO and further consumption of H_2 at the post flame zone.

At the lean burn zone, further ammonia and hydrogen are degraded to NH_2 and H radicals, respectively. Both H_2 and NH_3 consumption rate is increased at the lean burn zone due to excess availability of oxygen, contributing to higher O and OH radicals' productions.

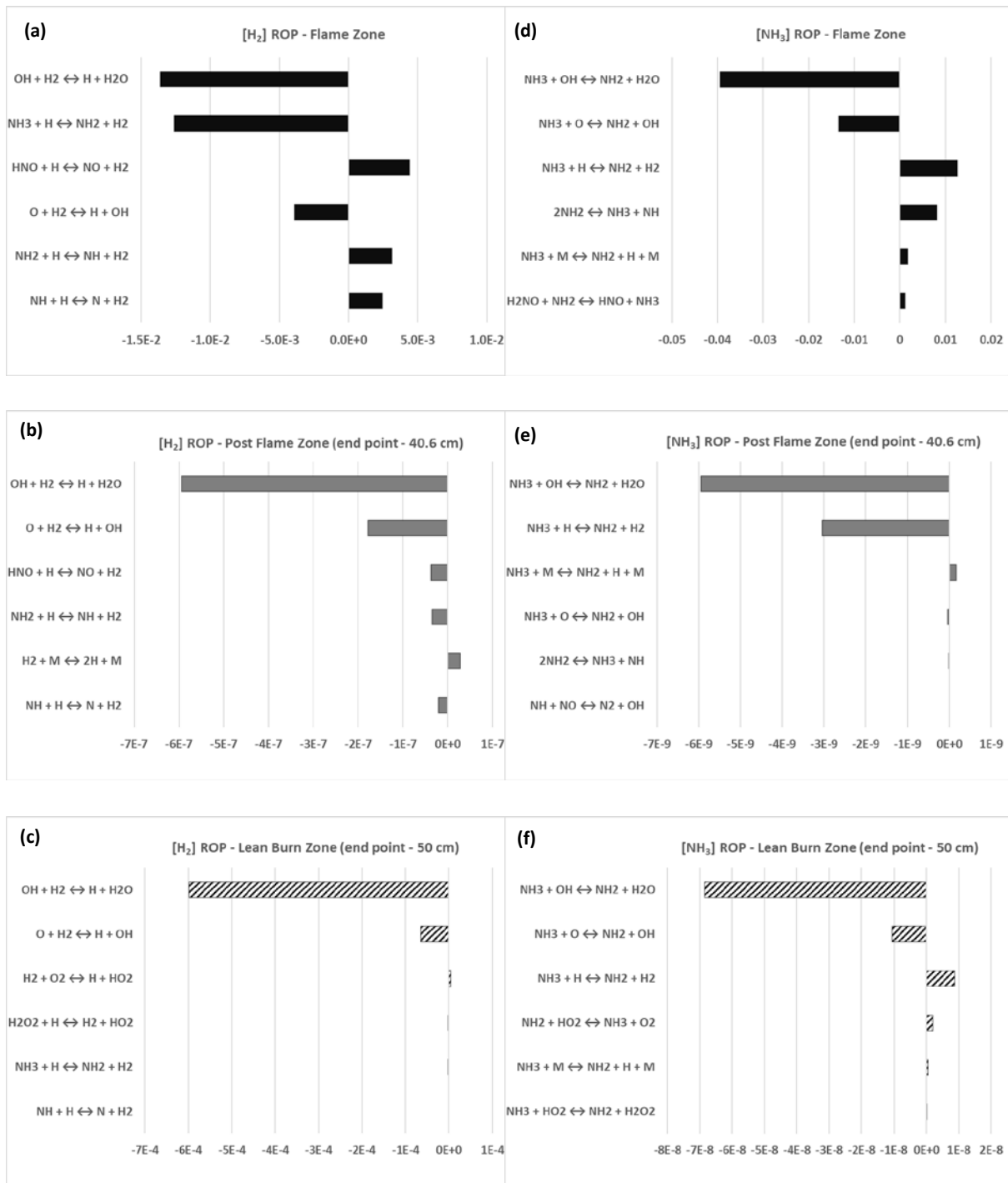


Fig 6. Computed absolute rate of production of [H₂] and [NH₃] at different locations of the RQL burner.

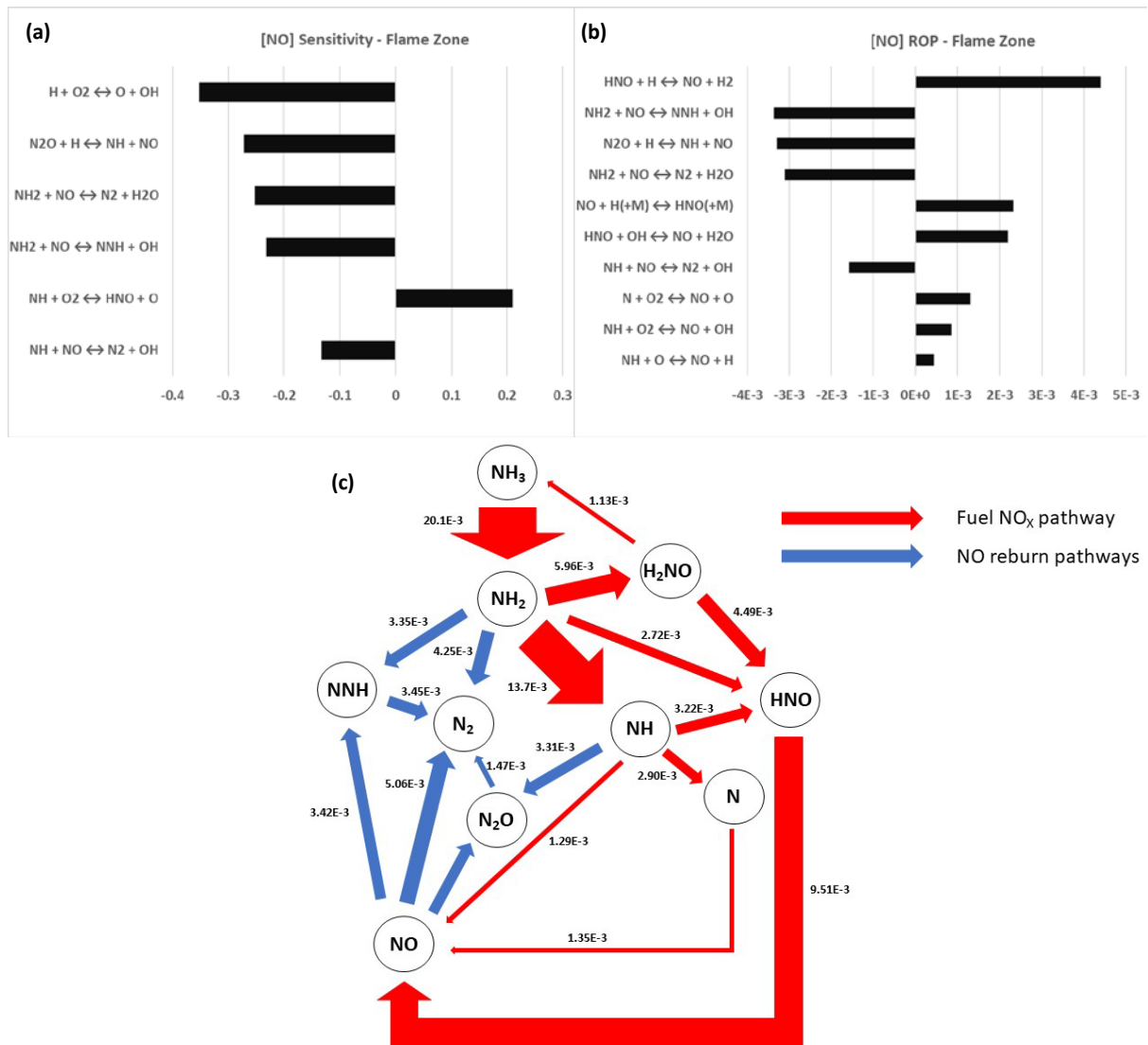


Fig 7. (a) Computed normalized sensitivity coefficients of [NO] on net reaction rates, (b) absolute rate of production of [NO], and (c) quantitative reaction path diagram of NO formation at the rich flame zone.

Next, detailed [NO] sensitivity analysis has been conducted with the aids of Quantitative Reaction Path Diagram (QRPD) and absolute ROP. Fig. 7 details the sensitivity coefficients, absolute ROP and QRPD of NO formation at the rich flame zone. As described earlier, the process initiates by NH_3 reacting with O and OH radicals to produce NH_2 radicals. Thus, the reaction $H + O_2 \leftrightarrow O + OH$ displays highest sensitivity for [NO] at the flame zone, Fig. 7(a). In turn, NH_2 converts to HNO through three different routes. First, directly through the reaction $NH_2 + O \leftrightarrow HNO + H$. Secondly, via H_2NO through the reaction $NH_2 + HO_2 \leftrightarrow H_2NO + OH$, and then H_2NO produces HNO by reacting with H, O, OH and NH_2 radicals. Finally, through the route $NH_2 > NH > HNO$. NH_2 converts to NH by reacting with H, O and OH radicals and through the decomposition reaction $2NH_2 \leftrightarrow NH_3$

+ NH. And then NH reacts with O₂ and OH radicals to produce HNO. Major source of NO at the flame zone is from HNO through the reactions $\text{HNO} + \text{H} \leftrightarrow \text{NO} + \text{H}_2$, $\text{HNO}(+\text{M}) \leftrightarrow \text{NO} + \text{H}(+\text{M})$ and $\text{HNO} + \text{OH} \leftrightarrow \text{NO} + \text{H}_2\text{O}$, Fig. 7(b). Substantial amount of NO is also formed from NH due to the reaction with O₂ and O radicals. NH also helps forming NO via atomic N formation. NH converts to N by reacting with H, OH and NH₂ radicals, and in turn N produces NO by reacting with the available oxygen at the flame zone.

Most of the NO produced in the flame zone burns out following different pathways. NO converts to stable molecular nitrogen through the reactions $\text{NH}_2 + \text{NO} \leftrightarrow \text{N}_2 + \text{H}_2\text{O}$; $\text{NH} + \text{NO} \leftrightarrow \text{N}_2 + \text{OH}$ and $\text{N} + \text{NO} \leftrightarrow \text{N}_2 + \text{O}$. NO also converts to NNH and N₂O by reacting with NH₂ and NH radicals, respectively, Fig. 7(b) and (c). Finally, NNH and some of the N₂O converts to stable N₂ by reacting with O₂ and H radicals, respectively.

Fig. 8 depicts NO formation/decomposition pathways and the most important reactions at the post flame zone. It is clear from Fig. 8 and Table 2 that most of the NO formed in the flame zone gets burnt away at the post flame zone. Contrary to the flame zone, NO converts to HNO at high temperature in the post flame zone through the reactions $\text{NO} + \text{H}(+\text{M}) \leftrightarrow \text{HNO}(+\text{M})$; $\text{HNO} + \text{H} \leftrightarrow \text{NO} + \text{H}_2$ and $\text{HNO} + \text{OH} \leftrightarrow \text{NO} + \text{H}_2\text{O}$. Interestingly, the last two reactions operate backwards at high temperature. Substantial amount of NO reacts with H radicals to produce N and OH radicals, Fig. 8(b). In turn HNO and atomic N react with H radicals and molecular hydrogen, respectively to form NH, which reacts with NO to form N₂O through the reaction $\text{NH} + \text{NO} \leftrightarrow \text{N}_2\text{O} + \text{H}$. Subsequently, NO reacts with atomic nitrogen, NH and NH₂ radicals to form stable N₂. NO also converts to N₂ via NNH through the reactions $\text{NH}_2 + \text{NO} \leftrightarrow \text{NNH} + \text{OH} \gg \text{NNH} \leftrightarrow \text{N}_2 + \text{H}$. Substantial amount of N₂ is also formed by burning NH₃ at the post flame zone through the route $\text{NH}_3 > \text{NH}_2 > \text{NNH} > \text{N}_2$.

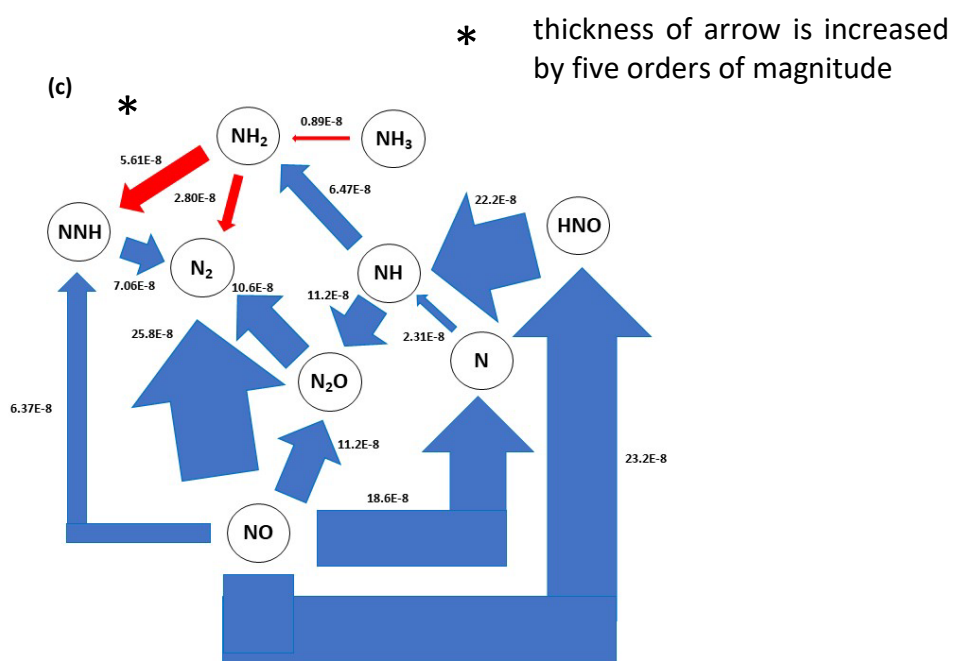
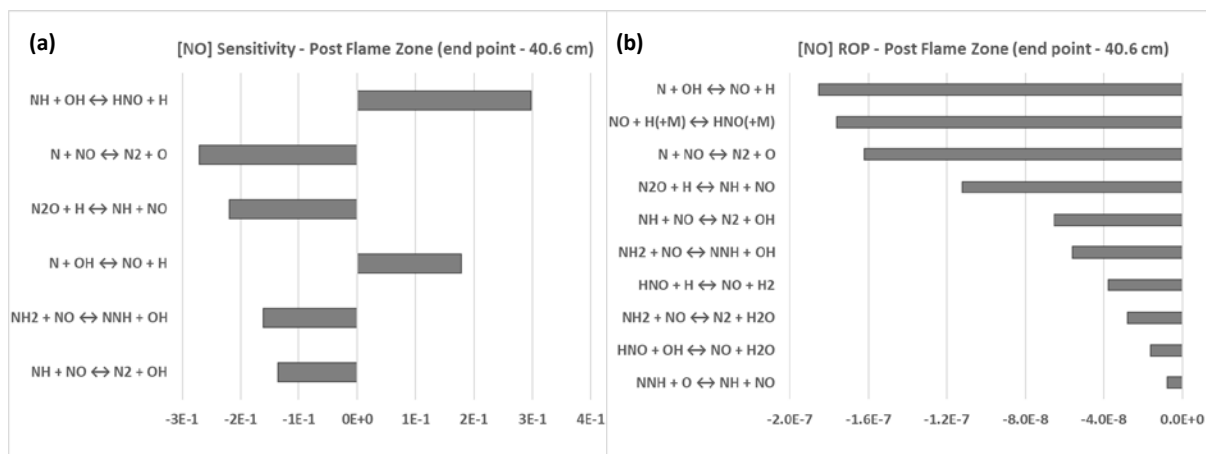


Fig 8. (a) Computed normalized sensitivity coefficients of [NO] on net reaction rates, (b) absolute rate of production of [NO], and (c) quantitative reaction path diagram of NO formation at the end point of post flame zone.

Next, NO formation/reburn pathways at the quenching/mixing zone are analysed, Fig. 9. Small amount of NO is formed at the quenching/mixing zone by burning small amount of ammonia through the fuel NO_x pathway, $\text{NH}_3 > \text{NH}_2 > \text{NH} > \text{N} > \text{NO}$. However, substantial amount of NO is burnt away at this zone according to Table 2 and Fig. 9(b). It must be noted that NO reburn arrows ($\text{NO} \rightarrow \text{HONO}$ and $\text{NO} \rightarrow \text{HNO}$) in Fig. 9(b) has an order of magnitude lower thickness than NO formation arrows. Therefore, lot more NO is burnt here than formed. The third body reaction $\text{NO} + \text{OH}(+M) \leftrightarrow \text{HONO}(+M)$ converts sizeable amount of NO to HONO, Fig. 9(a). Further NO is converted to HNO through another third body reaction $\text{NO} + \text{H}(+M) \leftrightarrow \text{HNO}(+M)$.

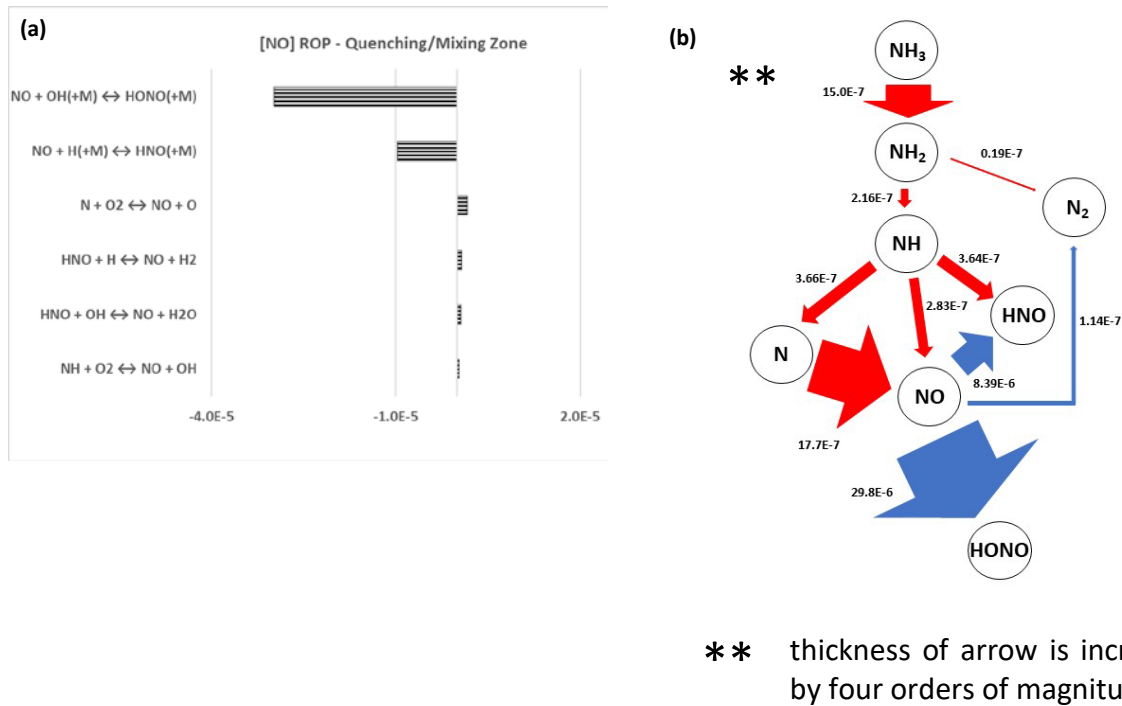


Fig 9. (a) Absolute rate of production of [NO], and (c) quantitative reaction path diagram of NO formation at the quenching/mixing zone. The thickness of arrow is increased by three orders of magnitude for $\text{NO} \rightarrow \text{HONO}$ and $\text{NO} \rightarrow \text{HNO}$.

Finally, NO formation/reburn pathways are analysed at the lean burn zone with the presence of excess oxygen, Fig. 10. Due to the presence of excess O_2 the third body reaction $\text{H} + \text{O}_2(+M) \leftrightarrow \text{HO}_2(+M)$ displays highest sensitivity for [NO] at the lean burn zone. Considerable amount of N_2O is formed through the reaction $\text{N}_2\text{O}(+M) \leftrightarrow \text{N}_2 + \text{O}(+M)$ operating at reverse direction. The third body reaction $\text{NO} + \text{H}(+M) \leftrightarrow \text{HNO}(+M)$ converts NO to HNO, while HNO reacts with O_2 and O radicals to form NO. Overall, more HNO is converted to NO due to lean burning. Sizeable amount of NO is converted to NO_2 by reacting with hydroperoxyl radicals. Subsequently, NO_2 reacts with HO_2 , H radicals and remaining hydrogen to convert to HONO, which contrary to the mixing/quenching zone, in turn forms further NO through the third body reaction $\text{NO} + \text{OH}(+M) \leftrightarrow \text{HONO}(+M)$ operating in the reverse direction. It must be noted that thickness of arrow is decreased by an order of magnitude for $\text{HONO} \rightarrow \text{NO}$, $\text{NO} \rightarrow \text{NO}_2$, and $\text{NO}_2 \rightarrow \text{HONO}$. Therefore, lot more NO is converted to NO_2 at the lean burn zone, compared to NO formation, as evidenced in Table 2.

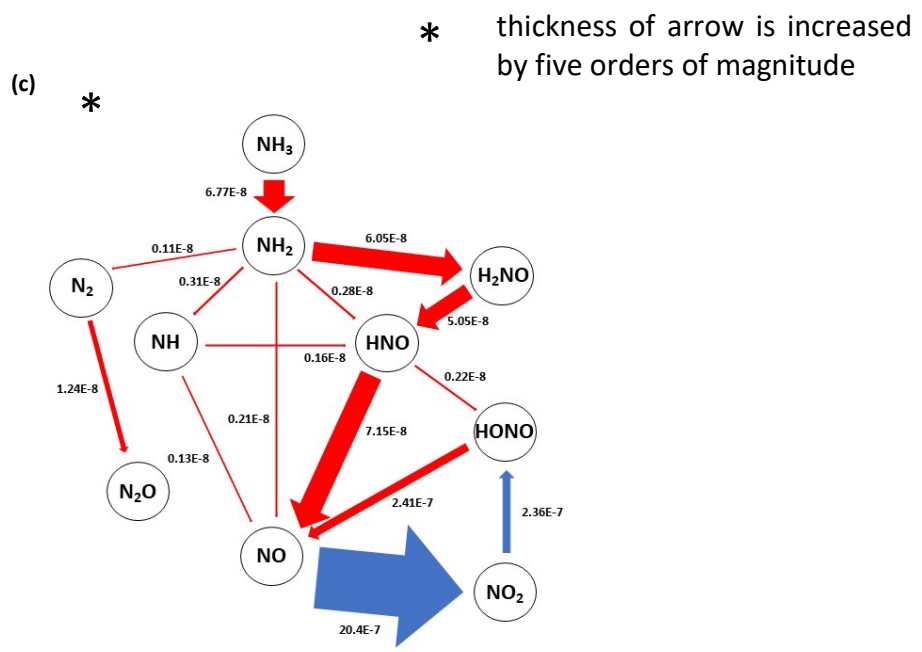
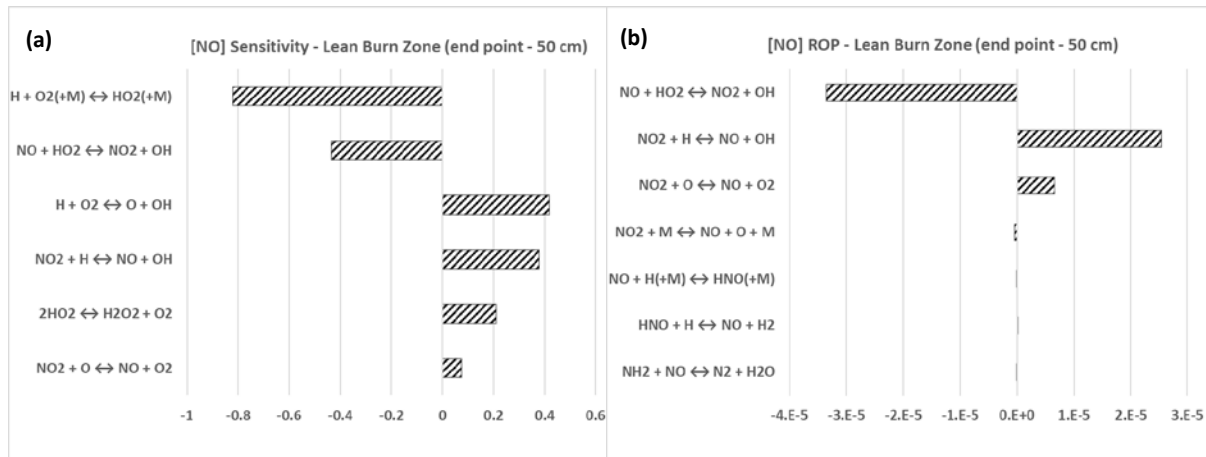


Fig 10. (a) Computed normalized sensitivity coefficients of [NO] on net reaction rates, (b) absolute rate of production of [NO], and (c) quantitative reaction path diagram of NO formation at the end point of lean burn zone. The thickness of arrow is increased by four orders of magnitude for HONO → NO, NO → NO₂, and NO₂ → HONO.

3.2. Trigeration Cycle Analysis

The results for Xiao mechanism were employed to calculate the efficiency of the trigeration cycle as previously stated. The first task in the analysis of the cycle was to determine the power output of the first gas turbine in Brayton cycle. Results from the first Brayton cycle predict turbine inlet temperatures of 1265K and an output power of 1490 kWe. Outlet temperatures at the first turbine exhaust are ~852 K. The first Brayton cycle's analyses showed that a basic humidified ammonia-hydrogen Brayton cycle can produce total plant efficiencies of ~34%, which is highly competitive to real case of the natural gas

fuelled gas turbine with maximum thermal efficiency of 36.45% [65]. Therefore, the second Brayton cycle (reversed Brayton cycle) was analysed with a second turbine inlet temperature of 852 K, delivering additional 530 kWe. The excess heat power produced in the process after accounting for the energy requirements to prepare the fuel and steam was estimated at ~4970 kWth (i.e. for district heating and industry). The required power for the steam pump was set at 110 kWe. In the trigeneration process, liquid ammonia is preheated in two steps (by air before the compressor and by hot nitrogen from the second compressor). The heat for ammonia preheating is obtained from the excess heat in the cycle. After splitting, additional heat needed for raising hydrogen temperature (i.e. from 288 to 588K) was determined at 60kWth. After including all losses in the process (mechanical losses, power for pumps, losses during transfer of the heat, flow and losses during transformation of the energy), the efficiency of the two shaft gas turbine plant with steam recirculation, fuel preheating and air cooling at the compressor inlet is estimated at ~59%.

Therefore, total efficiency values show a significant potential for the utilisation of humidified ammonia-based blends implemented in trigeneration power cycles that employ gas turbine technologies, especially compared to cogeneration systems including natural gas fuelled gas turbines with 50.50% real state efficiency and 60-70% for the theoretical case [65]. The obtained results highlight the opportunity for using these humidified ammonia-hydrogen blends for energy production in newly developed cycles which consider lower dilution in the combustion section, with competitive efficiency through cogeneration and trigeneration concepts, as presented in Figure 11. Humidified ammonia – hydrogen blend implemented in trigeneration power cycles with RQL technology can deliver higher efficiencies than combined Rankine Cycles with Organic Rankine Cycles/GTs with 47.65% efficiency. On the other hand, it must be emphasised that there are systems with higher efficiency, such as CHP concepts with internal combustion (IC) engines and rORC, systems that can reach efficiencies up to 60%. Furthermore, there are some CCHP systems with HSRG that can achieve efficiencies as high as 85%, although these systems are still reliant on carbon-based fuels. Nevertheless, this analysis shows that ammonia based cycles can be as competitive as other traditional cycles. However, there are still space for improvement to achieve higher efficiencies, as pointed out by the scope of this paper.

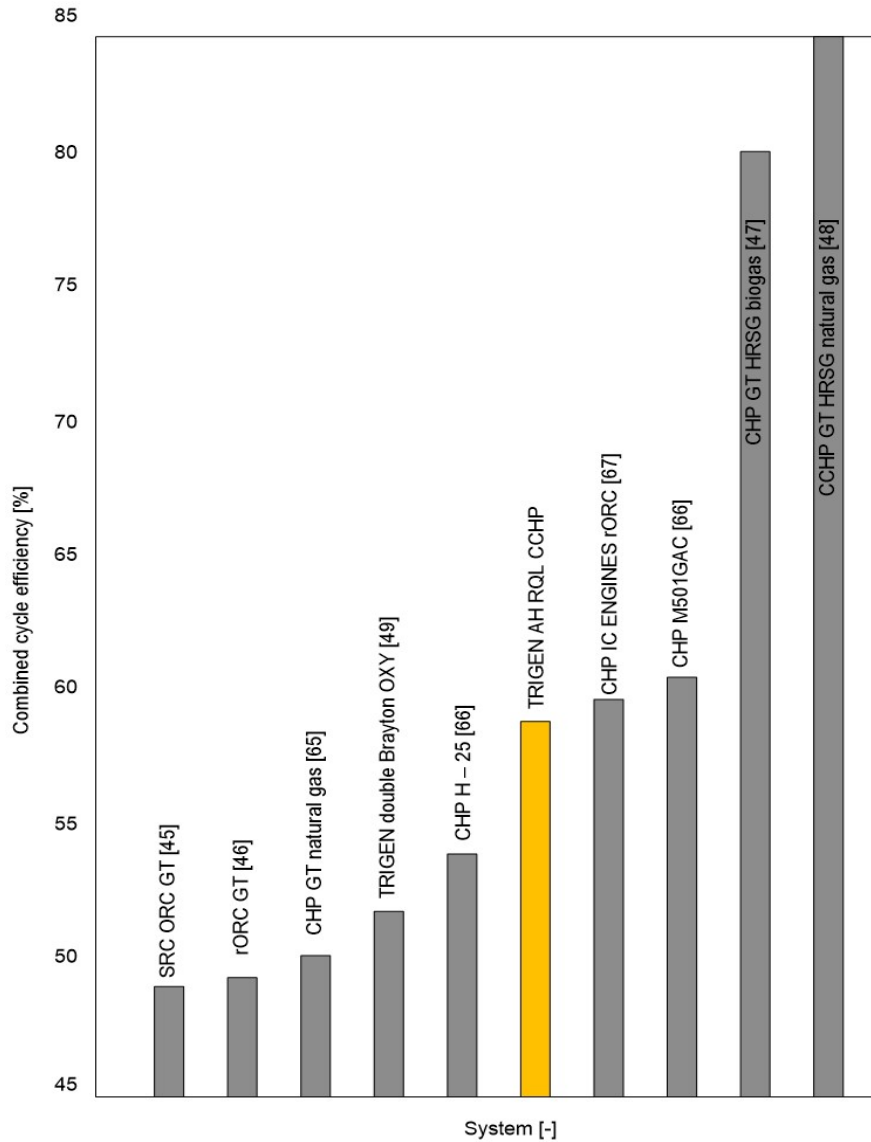


Fig 11. Comparison of the combined cycle efficiency for different traditional and new systems

4. Conclusion

A numerical and analytical analysis was performed in order to inspect the efficiency and potential to implement humidified ammonia-based blends in a two-shaft gas turbine plant with steam recirculation, fuel preheating and air cooling. The main purpose of the present analysis was the determination of the parameters of operating regimes which are competitive to current CHP and CCHP cycles operating with fossil fuels.

The radicals responsible for flame stability, namely H, O and OH radicals shown to have high sensitivity at the flame front, therefore high production/consumption rate. However, sensitivity of these radicals

reduces at the post flame zone due to the reduced availability of oxygen. Production/consumption of these radicals increases by a factor of ~ 3 at the lean burn zone, where remaining unburnt fuel burns away in the presence of excess oxygen. Numerical analysis predicted significant amount of NO production at the flame front through fuel bound NO pathway but most of these NO burns away at the post flame zone due to high temperature. However, sizable amount of N_2O was formed at this zone due to the reaction between NO and NH radicals. At the lean burn zone, considerable amount of NO converts to NO_2 by reacting with hydroperoxyl radicals.

Theoretical combustion results show the production of vast amounts of water with minimal traces of emissions across the post-combustion process. Pollutant emissions, i.e. NO_x and N_2O , in combination with unburned traces of ammonia, are only a minor fraction of the products in the flue gases entering the turbine. Although the concentration of these species tends to decrease across the combustor due to their high reactivity at high temperatures, it must be emphasised that there is still an issue that needs further development in terms of ammonia/hydrogen reactivity, with models that predict different results. However, the use of an RQL system demonstrate high performance in the considered scenario, with consumption of most reactive species and the production of NO_x emissions ~ 80 ppm, below current European NO_x thresholds.

Analyses on the cycle depicted that the use of a two-shaft gas turbine system with recirculated steam, fuel preheating and cooled inlet air was capable of delivering efficiencies $\sim 59\%$. This is a competitive efficiency to current fossil fuel based cycles, having in mind that no CO_2 emissions are produced, stranded renewable energy is efficiently employed as backup power with minimum chemical reconversion (i.e. back to 100% hydrogen) and parallel streams (N_2 and steam) employed to support further heating applications, thus increasing further the overall efficiency of this cycle.

5. Acknowledgment

This work was supported at Cardiff University by EPSRC, UKRI, project no. EP/T009314/1 “Stored Ammonia For Energy (SAFE)”. Information on the data underpinning the results presented here, including how to access them, can be found in the Cardiff University data catalogue at [DOI XXXXXXXX](#).

References

- [1] ‘The Future of Hydrogen – Executive Report’. International Energy Agency, 2019, Accessed: Jun. 23, 2020. [Online]. Available: <https://www.iea.org/reports/the-future-of-hydrogen>.
- [2] A. Valera-Medina, H. Xiao, M. Owen-Jones, W. I. F. David, and P. J. Bowen, ‘Ammonia for power’, *Prog. Energy Combust. Sci.*, vol. 69, pp. 63–102, 2018.

- [3] L. Haar, 'Thermodynamic properties of ammonia as an ideal gas', *J. Res. Natl. Bur. Stand. Sect. Phys. Chem.*, vol. 72, no. 2, p. 207, 1968.
- [4] E. Thorin, 'Thermophysical Properties of Ammonia–Water Mixtures for Prediction of Heat Transfer Areas in Power Cycles', *Int. J. Thermophys.*, vol. 22, no. 1, pp. 201–214, Jan. 2001, doi: 10.1023/A:1006745100278.
- [5] O. Elishav *et al.*, 'Progress and Prospective of Nitrogen-Based Alternative Fuels', *Chem. Rev.*, Jun. 2020, doi: 10.1021/acs.chemrev.9b00538.
- [6] J. Otomo, M. Koshi, T. Mitsumori, H. Iwasaki, and K. Yamada, 'Chemical kinetic modeling of ammonia oxidation with improved reaction mechanism for ammonia/air and ammonia/hydrogen/air combustion', *Int. J. Hydrog. Energy*, vol. 43, no. 5, pp. 3004–3014, 2018.
- [7] P. Glarborg, J. A. Miller, B. Ruscic, and S. J. Klippenstein, 'Modeling nitrogen chemistry in combustion', *Prog. Energy Combust. Sci.*, vol. 67, pp. 31–68, 2018.
- [8] R. C. da Rocha, M. Costa, and X.-S. Bai, 'Chemical kinetic modelling of ammonia/hydrogen/air ignition, premixed flame propagation and NO emission', *Fuel*, vol. 246, pp. 24–33, 2019.
- [9] E. R. Morgan, J. F. Manwell, and J. G. McGowan, 'Sustainable ammonia production from US offshore wind farms: a techno-economic review', *ACS Sustain. Chem. Eng.*, vol. 5, no. 11, pp. 9554–9567, 2017.
- [10] D. R. MacFarlane *et al.*, 'A Roadmap to the Ammonia Economy', *Joule*, vol. 4, no. 6, pp. 1186–1205, Jun. 2020, doi: 10.1016/j.joule.2020.04.004.
- [11] C. Zamfirescu and I. Dincer, 'Using ammonia as a sustainable fuel', *J. Power Sources*, vol. 185, no. 1, pp. 459–465, Oct. 2008, doi: 10.1016/j.jpowsour.2008.02.097.
- [12] C. Lhuillier, P. Brequigny, F. Contino, and C. Mounaïm-Rousselle, 'Experimental study on ammonia/hydrogen/air combustion in spark ignition engine conditions', *Fuel*, vol. 269, p. 117448, 2020.
- [13] Y. Niki, Y. Nitta, H. Sekiguchi, and K. Hirata, 'Diesel fuel multiple injection effects on emission characteristics of diesel engine mixed ammonia gas into intake air', *J. Eng. Gas Turbines Power*, vol. 141, no. 6, 2019.
- [14] P. Dimitriou and R. Javaid, 'A review of ammonia as a compression ignition engine fuel', *Int. J. Hydrog. Energy*, vol. 45, no. 11, pp. 7098–7118, 2020.
- [15] N. C. Kailos, *Utilization of ammonia as an alternate fuel in army aircraft engines*, vol. 66. US Army Aviation Materiel Laboratories, 1966.
- [16] M. G. Bull, 'Development of an ammonia-burning gas turbine engine', Solar Turbines International San Diego CA, 1968.
- [17] S. Colson *et al.*, 'Experimental and Numerical Study of NH₃/CH₄ Counterflow Premixed and Non-premixed Flames for Various NH₃ Mixing Ratios', *Combust. Sci. Technol.*, vol. 0, no. 0, pp. 1–18, May 2020, doi: 10.1080/00102202.2020.1763326.

- [18] A. Valera-Medina *et al.*, ‘Ammonia–methane combustion in tangential swirl burners for gas turbine power generation’, *Appl. Energy*, vol. 185, pp. 1362–1371, Jan. 2017, doi: 10.1016/j.apenergy.2016.02.073.
- [19] S. G. Hewlett, A. Valera-Medina, D. G. Pugh, and P. J. Bowen, ‘Gas turbine co-firing of steelworks ammonia with coke oven gas or methane: A fundamental and cycle analysis’, in *Turbo Expo: Power for Land, Sea, and Air*, 2019, vol. 58608, p. V003T03A018.
- [20] A. Valera-Medina *et al.*, ‘Premixed ammonia/hydrogen swirl combustion under rich fuel conditions for gas turbines operation’, *Int. J. Hydrog. Energy*, vol. 44, no. 16, pp. 8615–8626, Mar. 2019, doi: 10.1016/j.ijhydene.2019.02.041.
- [21] M. Guteša Božo, M. O. Vigueras-Zuniga, M. Buffi, T. Seljak, and A. Valera-Medina, ‘Fuel rich ammonia-hydrogen injection for humidified gas turbines’, *Appl. Energy*, vol. 251, p. 113334, Oct. 2019, doi: 10.1016/j.apenergy.2019.113334.
- [22] D. Pugh, P. Bowen, A. Valera-Medina, A. Giles, J. Runyon, and R. Marsh, ‘Influence of steam addition and elevated ambient conditions on NO_x reduction in a staged premixed swirling NH₃/H₂ flame’, *Proc. Combust. Inst.*, vol. 37, no. 4, pp. 5401–5409, 2019, doi: 10.1016/j.proci.2018.07.091.
- [23] H. Kobayashi, A. Hayakawa, K. K. A. Somarathne, and E. C. Okafor, ‘Science and technology of ammonia combustion’, *Proc. Combust. Inst.*, vol. 37, no. 1, pp. 109–133, 2019.
- [24] K. D. K. A. Somarathne *et al.*, ‘Emission characteristics of turbulent non-premixed ammonia/air and methane/air swirl flames through a rich-lean combustor under various wall thermal boundary conditions at high pressure’, *Combust. Flame*, vol. 210, pp. 247–261, 2019.
- [25] E. C. Okafor *et al.*, ‘Control of NO_x and other emissions in micro gas turbine combustors fuelled with mixtures of methane and ammonia’, *Combust. Flame*, vol. 211, pp. 406–416, Jan. 2020, doi: 10.1016/j.combustflame.2019.10.012.
- [26] M. Keller, M. Koshi, J. Otomo, H. Iwasaki, T. Mitsumori, and K. Yamada, ‘Thermodynamic evaluation of an ammonia-fueled combined-cycle gas turbine process operated under fuel-rich conditions’, *Energy*, 2020.
- [27] A. H. Lefebvre and D. R. Ballal, *Gas Turbine Combustion*, 3rd Editio. CRC Press, 2010.
- [28] J. Li, J. Chen, L. Yuan, G. Hu, and J. Feng, ‘Flow Characteristics of a Rich-Quench-Lean Combustor-Combined Low-Emission and High-Temperature Rise Combustion’, *Int. J. Aerosp. Eng.*, 2019, doi: 10.1155/2019/4014120.
- [29] B. Ge, Y. Ji, S. Zang, Y. Yuan, and J. Xin, ‘Investigation of the combustion performance in a three-nozzle RQL combustor’, 2016, doi: 10.1115/GT2016-57308.
- [30] K. D. K. A. Somarathne, S. Hatakeyama, A. Hayakawa, and H. Kobayashi, ‘Numerical study of a low emission gas turbine like combustor for turbulent ammonia/air premixed swirl flames with a secondary air injection at high pressure’, *Int. J. Hydrog. Energy*, vol. 42, no. 44, pp. 27388–27399, Nov. 2017, doi: 10.1016/j.ijhydene.2017.09.089.

- [31] P. Chiesa, G. Lozza, and L. Mazzocchi, 'Using hydrogen as gas turbine fuel', *J. Eng. Gas Turbines Power*, 2005, doi: 10.1115/1.1787513.
- [32] A. A. Taimoor, A. Muhammad, W. Saleem, and M. Zain-ul-abdein, 'Humidified exhaust recirculation for efficient combined cycle gas turbines', *Energy*, 2016, doi: 10.1016/j.energy.2016.03.079.
- [33] V. Shaposhnikov and B. Biryukov, 'Increasing efficiency of CCP-based TPP with injection of dry saturated steam from recovery boiler into regenerator', 2017, doi: 10.1088/1742-6596/891/1/012185.
- [34] W. De Paepe, M. Montero Carrero, S. Bram, F. Contino, and A. Parente, 'Waste heat recovery optimization in micro gas turbine applications using advanced humidified gas turbine cycle concepts', *Appl. Energy*, 2017, doi: 10.1016/j.apenergy.2017.06.001.
- [35] Z. Huang, C. Yang, H. Yang, and X. Ma, 'Off-design heating/power flexibility for steam injected gas turbine based CCHP considering variable geometry operation', *Energy*, 2018, doi: 10.1016/j.energy.2018.09.126.
- [36] C. Zhang, X. Wang, C. Yang, and Z. Yang, 'Control Strategies of Steam-injected Gas Turbine in CCHP System', 2017, doi: 10.1016/j.egypro.2017.03.461.
- [37] W. De Paepe, M. Renzi, M. M. Carrero, C. Caligiuri, and F. Contino, 'Micro gas turbine cycle humidification for increased flexibility: Numerical and experimental validation of different steam injection models', *J. Eng. Gas Turbines Power*, 2019, doi: 10.1115/1.4040859.
- [38] D. Xi, Y. Wang, J. Z. Liu, and J. H. Zhou, 'Current status in the study of the humidified combustion', *Reneng Dongli Gongcheng/Journal of Engineering for Thermal Energy and Power*. 2014.
- [39] Z. Huang, C. Yang, H. Yang, and X. Ma, 'Ability of adjusting heating/power for combined cooling heating and power system using alternative gas turbine operation strategies in combined cycle units', *Energy Convers. Manag.*, 2018, doi: 10.1016/j.enconman.2018.07.062.
- [40] Y. Zeting, L. Hai, H. Jitian, Z. Tao, and Y. Xiuyan, 'Performance analysis of a novel power/cooling cogeneration system with adjustable cooling-to-power ratio', *J. Eng. Thermophys.*, vol. 36, no. 2, pp. 254–258, 2015.
- [41] W. De Paepe, P. Sayad, S. Bram, J. Klingmann, and F. Contino, 'Experimental Investigation of the Effect of Steam Dilution on the Combustion of Methane for Humidified Micro Gas Turbine Applications', *Combust. Sci. Technol.*, 2016, doi: 10.1080/00102202.2016.1174116.
- [42] S. Shahpouri and E. Houshfar, 'Nitrogen oxides reduction and performance enhancement of combustor with direct water injection and humidification of inlet air', *Clean Technol. Environ. Policy*, 2019, doi: 10.1007/s10098-019-01666-4.
- [43] S. Göke and C. O. Paschereit, 'Influence of steam dilution on NO_x formation in premixed natural gas and hydrogen flames', 2012, doi: 10.2514/6.2012-1272.

- [44] A. K. Shukla and O. Singh, 'Performance evaluation of steam injected gas turbine based power plant with inlet evaporative cooling', *Appl. Therm. Eng.*, 2016, doi: 10.1016/j.applthermaleng.2016.03.136.
- [45] Ö. Köse, Y. Koç, and H. Yağlı, 'Performance improvement of the bottoming steam Rankine cycle (SRC) and organic Rankine cycle (ORC) systems for a triple combined system using gas turbine (GT) as topping cycle', *Energy Convers. Manag.*, vol. 211, p. 112745, 2020.
- [46] Y. Koç, H. Yağlı, and I. Kalay, 'Energy, Exergy, and Parametric Analysis of Simple and Recuperative Organic Rankine Cycles Using a Gas Turbine–Based Combined Cycle', *J. Energy Eng.*, vol. 146, no. 5, p. 04020041, 2020.
- [47] M. M. Guteša, B. D. Gvozdenac-Urošević, and V. R. Grković, 'Energy and economic effects of chp with combined technologies of corn cobs gasification and gas turbines', *Therm. Sci.*, 2016, doi: 10.2298/TSCI150925021G.
- [48] S. Popli, P. Rodgers, and V. Eveloy, 'Trigeneration scheme for energy efficiency enhancement in a natural gas processing plant through turbine exhaust gas waste heat utilization', *Appl. Energy*, 2012, doi: 10.1016/j.apenergy.2011.11.038.
- [49] P. Ziółkowski, W. Zakrzewski, O. Kaczmarczyk, and J. Badur, 'Thermodynamic analysis of the double Brayton cycle with the use of oxy combustion and capture of CO₂', *Arch. Thermodyn.*, 2013, doi: 10.2478/aoter-2013-0008.
- [50] M. Guteša Božo, A. Valera-Medina, N. Syred, and P. J. Bowen, 'Fuel quality impact analysis for practical implementation of corn COB gasification gas in conventional gas turbine power plants', *Biomass Bioenergy*, 2019, doi: 10.1016/j.biombioe.2019.01.012.
- [51] R. J. Kee, J. F. Grcar, M. D. Smooke, J. A. Miller, and E. Meeks, 'PREMIX: a Fortran program for modeling steady laminar one-dimensional premixed flames', *Sandia Natl. Lab. Rep.*, no. SAND85-8249, 1985.
- [52] S. Gordon and B. J. McBride, 'Computer program for calculation of complex chemical equilibrium compositions rocket performance incident and reflected shocks, and Chapman-Jouguet detonations', *Comput. Program Calc. Complex Chem. Equilib. Compos. Rocket Perform. Incid. Reflected Shocks ChapmanJouguet Detonations*, 1971.
- [53] H. Xiao and A. Valera-Medina, 'Chemical Kinetic Mechanism Study on Premixed Combustion of Ammonia/Hydrogen Fuels for Gas Turbine Use', *J. Eng. Gas Turbines Power*, vol. 139, no. 8, p. 081504, 2017, doi: 10.1115/1.4035911.
- [54] D. Pugh *et al.*, 'An investigation of ammonia primary flame combustor concepts for emissions reduction with OH*, NH₂* and NH* chemiluminescence at elevated conditions', *Proc. Combust. Inst.*, 2020.

- [55] D. Pugh *et al.*, ‘EMISSIONS PERFORMANCE OF STAGED PREMIXED AND DIFFUSION COMBUSTOR CONCEPTS FOR AN NH₃/AIR FLAME WITH AND WITHOUT REACTANT HUMIDIFICATION’.
- [56] M. Viguera-Zuniga, M. Tejada-del-Cueto, J. Vasquez-Santacruz, A. Herrera-May, and A. Valera-Medina, ‘Numerical Predictions of a Swirl Combustor Using Complex Chemistry Fueled with Ammonia/Hydrogen Blends’, *Energies*, vol. 13, no. 2, p. 288, 2020, doi: doi.org/10.3390/en13020288.
- [57] A. Valera-Medina, N. Syred, and P. Bowen, ‘Central recirculation zone visualization in confined swirl combustors for terrestrial energy’, *J. Propuls. Power*, vol. 29, no. 1, 2013, doi: 10.2514/1.B34600.
- [58] S. Mashruk, ‘NO Formation Analysis using Chemical Reactor Modelling and LIF Measurements on Industrial Swirl Flames’, PhD Thesis, Cardiff University, 2020.
- [59] A. Valera-Medina, A. Giles, D. Pugh, S. Morris, M. Pohl, and A. Ortwein, ‘Investigation of Combustion of Emulated Biogas in a Gas Turbine Test Rig’, *J. Therm. Sci.*, 2018, doi: 10.1007/s11630-018-1024-1.
- [60] F. J. Verkamp, M. C. Hardin, and J. R. Williams, ‘Ammonia combustion properties and performance in gas-turbine burners’, in *Symposium (International) on Combustion*, 1967, vol. 11, no. 1, pp. 985–992.
- [61] A. Al-Doboan, M. Gutesa, A. Valera-Medina, N. Syred, J.-H. Ng, and C. T. Chong, ‘CO₂-argon-steam oxy-fuel (CARSOXY) combustion for CCS inert gas atmospheres in gas turbines’, *Appl. Therm. Eng.*, vol. 122, 2017, doi: 10.1016/j.applthermaleng.2017.05.032.
- [62] M. Gutesa, ‘The Numerical Simulation Model of Gas Turbine Facility for Biomass Gasification Gas Application’, PhD Thesis, Novi Sad University, 2017.
- [63] M. Gutesa, A. Al-Doboan, A. Valera-Medina, N. Syred, and P. J. Bowen, ‘Carsoxy (CO₂-argon-steam-Oxyfuel) combustion in gas turbines for CCS systems’, 2017, doi: 10.2514/6.2017-1608.
- [64] British Standard, ‘BS ISO 11042-1:1996. Gas Turbines-Exhaust Gas Emission’, 1996.
- [65] Y. Koc, O. Kose, and H. Yagli, ‘Exergy analysis of a natural gas fuelled gas turbine based cogeneration cycle’, *Int. J. Exergy*, vol. 30, no. 2, pp. 103–125, 2019.
- [66] Mitsubishi Power, ‘GTCC Gas Turbine Combined Cycle Power Plants’, Accessed: Sep. 21, 2020. [Online]. Available: <https://power.mhi.com/catalogue/pdf/gtcc.pdf>.
- [67] M.J. Abedin, H.H. Masjuki, M.A. Kalam, A. Sanjid, S.A. Rahman, B.M. Masum, Energy balance of internal combustion engines using alternative fuels. *Renew. Sustain. Energy Rev*, Vol. 26, pp. 20–33, 2013.